Tensor-entanglement renormalization group approach as a unified method for symmetry breaking and topological phase transitions

Zheng-Cheng Gu,[1] Michael Levin,[2] and Xiao-Gang Wen[1]
[1]*Department of Physics, Massachusetts Institute of Technology, Cambridge, Massachusetts 02139, USA*
[2]*Department of Physics, Harvard University, Cambridge, Massachusetts 02138, USA*
(Received 24 June 2008; published 24 November 2008)

Traditional mean-field theory is a generic variational approach for analyzing symmetry breaking phases. However, this simple approach only applies to symmetry breaking states with short-range entanglement. In this paper, we describe a generic approach for studying two-dimensional (2D) quantum phases with long-range entanglement (such as topological phases). The method is based on (a) a general class of trial wave functions known as tensor-product states and (b) a 2D real-space renormalization group algorithm for efficiently calculating expectation values for these states. We demonstrate our method by studying several simple 2D quantum spin models exhibiting both symmetry breaking phase transitions and topological phase transitions. Our approach can be viewed as a unified mean-field theory for both symmetry breaking phases and topological phases.

DOI: 10.1103/PhysRevB.78.205116 PACS number(s): 75.10.−b, 64.70.Tg

I. INTRODUCTION

Landau's symmetry breaking theory[1,2] for phases and phase transitions is one of the foundations of condensed-matter theory. A central component of this framework is Ginzburg-Landau effective theory[3] or, more generally, mean-field theory. For $T=0$ quantum states, such a mean-field approach is actually a variational approach based on trial wave functions which are roughly direct product states. For example, to study the possible spin-ordered phases in spin-1/2 systems $H=\Sigma_{\langle ij\rangle}\boldsymbol{S}_i\cdot\boldsymbol{J}_{ij}\cdot\boldsymbol{S}_j$, we may start with a trial wave function $|\Psi_{\text{trial}}\rangle=\otimes(u_i|\uparrow\rangle_i+v_i|\downarrow\rangle_i)$, where $|\uparrow\rangle_i$ and $|\downarrow\rangle_i$ are spin states on site i. The different possible spin-ordered phases can be obtained by changing the order parameters u_i and v_i so as to minimize the average energy.

Although this simple mean-field approach cannot describe the quantitative properties of phases and phase transitions, it often captures the correct qualitative physics, such as possible symmetry breaking phases in a phase diagram, as well as the order of the phase transitions between different phases. Thus, the mean-field approach is conceptually important because it captures the physics behind symmetry breaking phases and phase transitions between them. Moreover, by applying perturbative methods based on the mean-field approach, we may quantitatively improve our results.

However, this kind of mean-field theory only applies to states with short-range entanglement. Even after including quantum fluctuations in the mean-field ansatz, it still cannot describe states with nonlocal long-range entanglement. As a result, we cannot use the traditional mean-field theory to calculate quantum phases (such as topologically ordered states[4]) that have a pattern of long-range entanglement[5] as revealed by nonzero topological entropy.[6,7] These kinds of phases are beyond Landau's symmetry breaking paradigm.

The key concept in the mean-field approach is that it describes a many-body quantum state through a set of *local* order parameters, such as u_i and v_i in spin-1/2 system. Although the total dimension of the Hilbert space scales exponentially with the total system size, the relevant low-energy states are characterized by a polynomially large set of *local* parameters. Thus, we can calculate the low-energy physical properties in a very simple and efficient way.

Motivated by the success of the mean-field theory for symmetry breaking phases, we would like to develop a "mean-field" theory for topologically ordered phases and phase transitions.[8–14] The main challenges in developing such a mean-field-like approach are (a) finding a class of states that can have the long-range entanglement found in topological phases and (b) finding a simple way to calculate the physical properties, such as average energy, of these states.

The first problem can be solved with a general class of trial wave functions known as "tensor-product states" (or alternatively "projected entangled pair states").[15–18] These states were first discovered in the context of the one-dimensional (1D) density-matrix renormalization group (DMRG) method[19,20] but were later generalized to higher dimensions and arbitrary lattices. One can show that tensor-product states (TPSs) can describe all the string-net condensed states constructed in Ref. 21 and hence all nonchiral topological phases.[22]

Given this fact, the second problem becomes: can we calculate expectation values of operators in a TPS efficiently? Consider the case of the square lattice (Fig. 1). On the square lattice, tensor-product states are defined by the following expression for the many-body wave function $\Psi(\{m_i\})$:

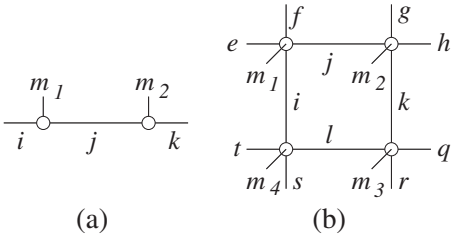

FIG. 1. Tensor network: a graphic representation of the tensor-product wave function (1), (a) on a 1D chain or (b) on a 2D square lattice. The indices on the links are summed over.

TABLE I. Error scaling for several variational approaches. T is the calculation time and ϵ is the achieved relative accuracy of the calculated average energy for a given many-body state. The acronym VQMC stands for variational quantum Monte Carlo, while "1D approach" refers to an approximation scheme where one replaces the infinite 2D lattice by an $L\times\infty$ lattice, for L large but finite, and then computes expectation values using a transfer-matrix approach (see the Appendix for a derivation).

Method	Error
VQMC	$\epsilon\sim 1/T^{1/2}$
1D approach	$\epsilon\sim\exp[-\text{const}(\log T)]$
TERG	$\epsilon\sim\exp[-\text{const}(\log T)^2]$

$$\Psi(\{m_i\})=\sum_{ijkl\cdots} T^{m_1}_{ejfi}T^{m_2}_{jhgk}T^{m_3}_{lqkr}T^{m_4}_{tlis}\cdots. \tag{1}$$

Here $T^{m_i}_{ejfi}$ is a complex tensor with one physical index m_i and four inner indices $i,j,k,l,\cdots$. The physical index runs over the number of physical states d on each site and the internal indices runs over D values. Beyond one dimension, it is not easy to compute expectation values in these states. Summing over all the internal indices is an exponentially long calculation.

In this paper, we describe a simple solution to this problem in two dimensions (2Ds). Our approach—which we call the tensor-entanglement renormalization group (TERG) method—is an approximation scheme based on the 2D real-space RG method described in Ref. 23. (A different real-space RG method can be found in Ref. 24.) The TERG method allows us to efficiently calculate the averages and correlations of local operators.

We can view the TERG approach as a variational approach. After calculating the average energy of a TPS using the TERG method, we can choose the tensor to minimize the average energy and hence obtain an approximate ground state. This allows us to obtain a mean-field phase diagram for quantum states that may contain both symmetry breaking phases and topological phases. In some sense, the TERG approach plays a role for topological phases like the Ginzburg-Landau theory for symmetry breaking phases.

Table I compares the efficiency of the TERG method with other variational methods for 2D gapped systems. We see that the TERG method is very efficient with $\epsilon\sim e^{-\text{const}(\log T)^2}$ error scaling.

The paper is organized as follows. In Sec. II we introduce the basic method. In Sec. III we demonstrate it with several spin models with symmetry breaking transitions. Finally, in Sec. IV we apply the method to spin models with topological phase transitions, revealing some of the additional subtleties that occur in this case.

II. TERG METHOD

A. TERG algorithm on square lattice

To describe the TERG method, let us consider a system with a translationally invariant Hamiltonian $H=\Sigma_i h_i$ where i labels the lattice sites. The h_i can always be expressed as a summation of products of local operators: $h_i=\hat{O}^0_i+\hat{O}^1_i\hat{O}^2_{j=NN(i)}+\cdots$ where $j=NN(i)$ is the next neighbor of i. A key step in the variational approach is to calculate the norm and the expectation value of h_i for the trial wave function $\Psi(\{m_i\})$,

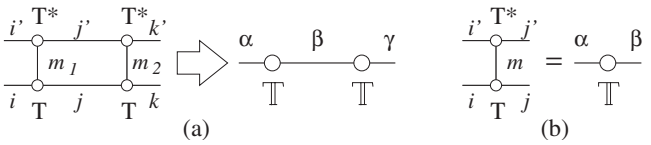

FIG. 2. (a) The graphic representation of the inner product of TPS $\langle\Psi|\Psi\rangle$ in term of the tensor T or the double tensor $\mathbb{T}$ [see Eq. (2)]. (b) After summing over m and identifying $(i,i')\to\alpha$ and $(j,j')\to\beta$, we obtain the double tensor $\mathbb{T}$ from T and T^*.

$$\langle\Psi|\Psi\rangle=\sum_{m_1m_2\cdots}\sum_{ii'jj'\cdots} T^{m_1}_{ejfi}T^{m_1*}_{e'j'f'i'}T^{m_2}_{jhgk}T^{m_2*}_{j'h'g'k'}\cdots$$
$$=\text{tTr}[\mathbb{T}\otimes\mathbb{T}\otimes\mathbb{T}\otimes\cdots],$$
$$\langle\Psi|h_i|\Psi\rangle=\text{tTr}[\mathbb{T}^0\otimes\mathbb{T}\otimes\mathbb{T}\otimes\cdots]+\text{tTr}[\mathbb{T}^1\otimes\mathbb{T}^2\otimes\mathbb{T}\otimes\cdots]$$
$$+\cdots, \tag{2}$$

where double tensors $\mathbb{T}$ and $\mathbb{T}^a$ $(a=0,1,2)$ are defined as [see Fig. 2(b)]

$$\mathbb{T}=\sum_m T^{m*}\otimes T^m;\quad \mathbb{T}^a=\sum_{mm'} O^a_{mm'}T^{m*}\otimes T^m \tag{3}$$

with $O^a_{mm'}$ as the matrix elements of local operators $\hat{O}^a$ in the local basis $|m\rangle$. The tensor trace (tTr) here means summing over all indices on the connected links of tensor network [see Fig. 3(a)]. Note that the inner product is obtained from a uniform tensor network. The average of the on-site interaction is obtained from a tensor network with one "impurity" tensor $\mathbb{T}^0$ at site i (while other site has $\mathbb{T}$). Similarly, for two-body interactions, the tensor network has two "impurity" tensors $\mathbb{T}^1$ and $\mathbb{T}^2$ at i and j.

Calculating the tTr is an exponentially hard calculation in 2D or higher dimensions. Motivated by the tensor-renormalization approach developed in Ref. 23, we can accelerate the calculation exponentially if we are willing to make an approximation. The basic idea is quite simple and is

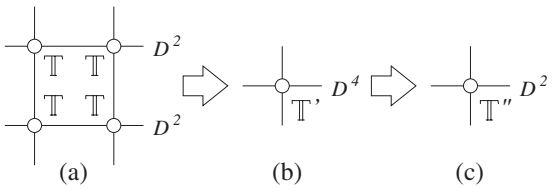

FIG. 3. The indices of the double tensor have a range D^2. After combining the two legs on each side into a single leg, the four-linked double tensors in (a) can be viewed as a single double tensor $\mathbb{T}'$ whose indices have a range D^4. (c) $\mathbb{T}'$ can be approximately reduced to a "smaller" double tensor $\mathbb{T}''$ whose indices have a range D^2 and satisfies $\text{t Tr}[\mathbb{T}'\otimes\mathbb{T}'\cdots]\approx\text{t Tr}[\mathbb{T}''\otimes\mathbb{T}''\cdots]$.

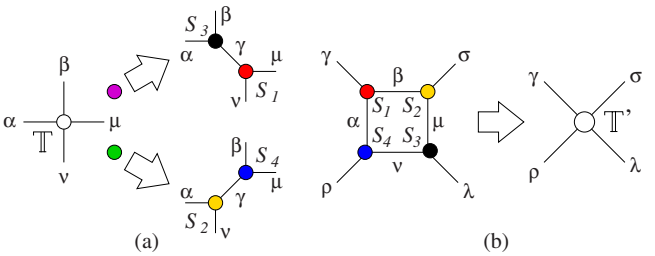

FIG. 4. (Color online) (a) We represent the original rank-four tensor by two rank-three tensors, which is an *approximate* decomposition. (b) Summing over the indices around the square produces a single tensor $\mathbb{T}'$. This step is *exact*.

illustrated in Fig. 3. After finding the reduced double tensor $\mathbb{T}''$, we can express $\mathrm{tTr}[\mathbb{T}\otimes\mathbb{T}\cdots]\approx\mathrm{tTr}[\mathbb{T}''\otimes\mathbb{T}''\cdots]$ where the second tensor trace only contains a quarter of the double tensors in the first tensor trace. We may repeat the procedure until there are only a few double tensors in the tensor trace. This allows us to reduce the exponentially long calculation to a polynomially long calculation.

The detailed implementation of the above TERG approach is actually a little more involved. For a uniform tensor network [Fig. 3(a)], we can coarse grain it in two steps. The first step is decomposing the rank-four tensor into two rank-three tensors. We do it in two different ways on the sublattice purple and green [see Fig. 4(a)]. On purple sublattice, we have $\mathbb{T}_{\alpha\beta\mu\nu}=\Sigma_{\gamma'}S_{1\mu\nu\gamma'}S_{3\alpha\beta\gamma'}$ and on green sublattice, we have $\mathbb{T}_{\alpha\beta\mu\nu}=\Sigma_{\gamma'}S_{2\nu\alpha\gamma'}S_{4\beta\mu\gamma'}$. Note that α, β, μ, and ν run over D^2 values while γ' run over D^4 values.

Next we try to reduce the range of γ' through an approximation.[23] Say, on purple sublattice, we view $\mathbb{T}_{\alpha\beta\mu\nu}$ as a matrix $M^{\mathrm{red}}_{\alpha\beta;\mu\nu}=\mathbb{T}_{\alpha\beta\mu\nu}$ and do a singular value decomposition (SVD) $M^{\mathrm{red}}=U\Lambda V^{\dagger}$. We then keep only the largest D_{cut} singular values λ_γ and define $S_{1\mu\nu\gamma}=\sqrt{\lambda_\gamma}V^{\dagger}_{\gamma,\mu\nu}$ and $S_{3\alpha\beta\gamma}=\sqrt{\lambda_\gamma}U_{\alpha\beta,\gamma}$. Thus, we can approximately express $\mathbb{T}_{\alpha\beta\mu\nu}$ by two rank-three tensors S_1 and S_3

$$\mathbb{T}_{\alpha\beta\mu\nu}\simeq\sum_{\gamma=1}^{D_{\mathrm{cut}}}S_{3\alpha\beta\gamma}S_{1\mu\nu\gamma}. \tag{4}$$

Similarly, on green sublattice we may also view $\mathbb{T}_{\alpha\beta\mu\nu}$ as a matrix $M^{\mathrm{green}}_{\nu\alpha;\beta\mu}$ and do a singular value decompositions, keep the largest D_{cut} singular values, and approximately express $\mathbb{T}_{\alpha\beta\mu\nu}$ by two rank-three tensors S_2 and S_4.

$$\mathbb{T}_{\alpha\beta\mu\nu}\simeq\sum_{\gamma=1}^{D_{\mathrm{cut}}}S_{2\nu\alpha\gamma}S_{4\beta\mu\gamma}. \tag{5}$$

After such decompositions, the square lattice is deformed into the form in Fig. 4(b) (see also Fig. 5). The second step is to simply contract the square and get a new tensor on the coarse-grained lattice,

$$\mathbb{T}'_{\gamma\sigma\lambda\rho}=\sum_{\alpha\beta\mu\nu}S_{1\beta\alpha\gamma}S_{2\mu\beta\sigma}S_{3\nu\mu\lambda}S_{4\alpha\nu\rho}. \tag{6}$$

The range of indices for the reduced double tensor $\mathbb{T}'$ is only D_{cut} which can be chosen to be D^2 or some other value. Repeating the above two steps twice, we can get the reduction from Figs. 3(a)–3(c). After n steps, we can reduce a system with 2^n lattice sites to a single coarse-grained site with a coarse-grained double tensor $\mathbb{T}^n$. The norm of our trial wave function $\Psi(\{m_i\})$ [under periodic boundary condition (PBC)] can be simply obtained by tracing out this double tensor,

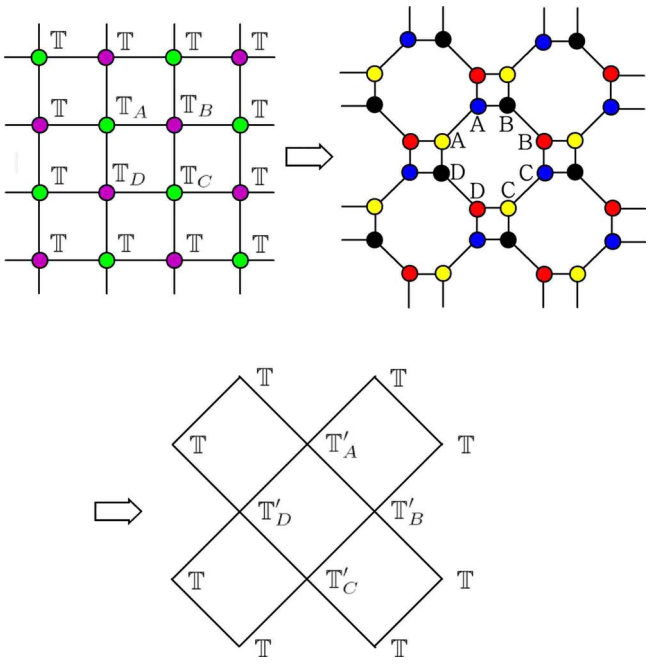

FIG. 5. (Color online) Under the TERG procedure, a tensor network is transformed into a coarse-grained tensor network.

$$\langle\Psi|\Psi\rangle=\sum_{\gamma\sigma}\mathbb{T}^n_{\gamma\sigma\gamma\sigma}. \tag{7}$$

The above TERG procedure is for a uniform tensor network where all the double tensors are the same. However, it can be easily generalized to a tensor network with "impurities," such as the one in Fig. 5 which has four "impurity" tensors. Evaluating Fig. 5 will allow us to calculate the averages of up to four-body nearest-neighbor interactions (which includes on-site interaction, nearest-neighbor, and next-nearest-neighbor two-body interactions). The TERG procedure is illustrated in Fig. 5. We note that the number and the relative positions of "impurity" tensors do not change after each iteration. So we can repeat the same iterative calculation until there are only a few tensors in the tensor trace.

Let us take the nearest-neighbor interaction term, for example. For the uniform double tensor $\mathbb{T}$, we can coarse grain it in the same way as what we do in calculating the norm. For the impurity double tensors $\mathbb{T}^1$ and $\mathbb{T}^2$, we can initialize the four impurity double tensors in Fig. 5 as $\mathbb{T}_A=\mathbb{T}^1$, $\mathbb{T}_B=\mathbb{T}^2$, $\mathbb{T}_C=\mathbb{T}$, and $\mathbb{T}_D=\mathbb{T}$. We put $\mathbb{T}_A$ and $\mathbb{T}_C$ on green sublattice and $\mathbb{T}_B$ and $\mathbb{T}_D$ on purple sublattice. We use the same decomposition rules for each sublattice and keep the largest D_{cut} singular values,

$$\mathbb{T}_{A(C)_{\alpha\beta\mu\nu}}\simeq\sum_{\gamma=1}^{D_{\mathrm{cut}}}S_{A(C)2_{\nu\alpha\gamma}}S_{A(C)4_{\beta\mu\gamma}} \tag{8}$$

and

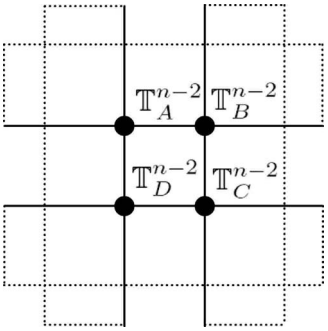

FIG. 6. The tensor trace of this simple tensor network gives us $\langle\Psi|\hat{O}_i^1\hat{O}_{j=NN(i)}^2|\Psi\rangle$. Again, the indices on connected links are summed over in the tensor trace.

$$\mathbb{T}_{B(D)_{\alpha\beta\mu\nu}} \simeq \sum_{\gamma=1}^{D_{\text{cut}}} S_{B(D)1_{\alpha\beta\gamma}} S_{B(D)3_{\mu\nu\gamma}}. \tag{9}$$

Then, we can sum over the indices on the links for each small square and produce the coarse-grained tensors. For example, $\mathbb{T}'_A$ can be calculated as

$$\mathbb{T}'_{A\gamma\sigma\lambda\rho} = \sum_{\alpha\beta\mu\nu} S_{1\beta\alpha\gamma} S_{2\mu\beta\sigma} S_{B3\nu\mu\lambda} S_{A4\alpha\nu\rho}. \tag{10}$$

$\mathbb{T}'_C$, $\mathbb{T}'_B$, and $\mathbb{T}'_D$ can be calculated in a similar way.

For a system with 2^n lattice sites, after coarse graining for $n-2$ times, we end up with only four impurity tensors T_A^{n-2}, $\mathbb{T}_B^{n-2}$, $\mathbb{T}_C^{n-2}$, and $\mathbb{T}_D^{n-2}$. Under PBC, to obtain the expectation value $\langle\Psi|\hat{O}_i^1\hat{O}_{j=NN(i)}^2|\Psi\rangle$, we only need to truncate the four impurity tensors in the way as shown in Fig. 6

$$\langle\Psi|\hat{O}_i^1\hat{O}_{j=NN(i)}^2|\Psi\rangle = \text{t Tr}[\mathbb{T}_A^{n-2} \otimes \mathbb{T}_B^{n-2} \otimes \mathbb{T}_C^{n-2} \otimes \mathbb{T}_D^{n-2}].$$

Thus the calculation of the averages of local operators is also reduced to a polynomially long calculation. The total computational complexity is: cost time $\sim D_{\text{cut}}^6 \log N$ on square lattice (N is the total number of sites). For gapped systems in the thermodynamic limit, the truncation error can be estimated as $\epsilon \sim \exp[-\text{const}(\log D_{\text{cut}})^2]$.[23] After calculating the inner product and the average of h_i in Eq. (2), we can obtain the approximate ground state with minimized average energy by adjusting the elements in the tensor T.

B. Correlation functions through the TERG method

The correlation functions of two operators with arbitrary separations for a given TPS can also be calculated in a similar way. In the following, we assume $|\mathbf{r}_j - \mathbf{r}_i| = L = 2^m$ and use this simple example to show how the method works. The two-body correlation functions $\langle\Psi|\hat{O}_i\hat{O}_j|\Psi\rangle$ can be represented as a tensor trace with two impurity double tensors live on sites i and j and with uniform double tensors $\mathbb{T}$ on other sites, as shown in Fig. 7(a). After one step of coarse graining (we shrink the shaded region in Fig. 7(a) to a point when doing coarse graining), we obtain a tensor network in Fig. 7(b). Notice the impurity tensors increase to two in each plaquette and the distance between them becomes $L/\sqrt{2}$. After two more steps of coarse graining, the number of impurity tensors increases to four in each plaquette but the distance between them becomes $L/2\sqrt{2}$, as shown in Figs. 7(c) and 7(d). However, after increasing to four impurity tensors in a plaquette, the number of impurity tensors will not increase in subsequent coarse graining procedures, as shown in Fig. 7(e). Finally, if L is equal to the half of the linear system size ($L = \sqrt{N}/2$), we can end up with a tensor network where two impurity-tensor plaquettes touch each other, as shown in Fig. 7(f). Under PBC, after truncating the up and down legs and left and right legs of this tensor net, we obtain the two-body correlation functions in this case. In more generic cases $L < \sqrt{N}/2$, we need to do more steps of coarse graining starting from the configuration in Fig. 7(e). As in Fig. 8, we can do a series of coarse graining steps from Figs. 8(a)–8(f). However, Fig. 8(f) will come back to the case shown in Fig. 8(c) after one step of coarse graining and thus we do not need to consider other possible configurations. In conclusion, for an arbitrary m in $|\mathbf{r}_i - \mathbf{r}_j| = 2^m$, we may stop at a configuration from Figs. 8(a)–8(f). Under PBC, we can obtain the correlation function by performing the tensor trace on the resulting tensor network.

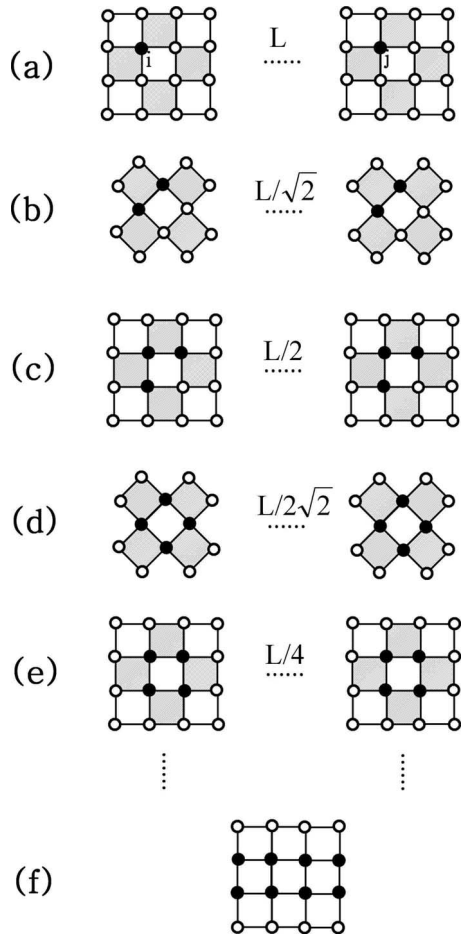

FIG. 7. A schematic plot of calculating a two-body correlation functions with separation $|\mathbf{r}_j - \mathbf{r}_i| = L = 2^m$ assuming $L = \sqrt{N}/2$. The solid dots represent the impurity tensors and open dots represent the uniform tensors. We shrink the shaded region to a single point when doing coarse graining.

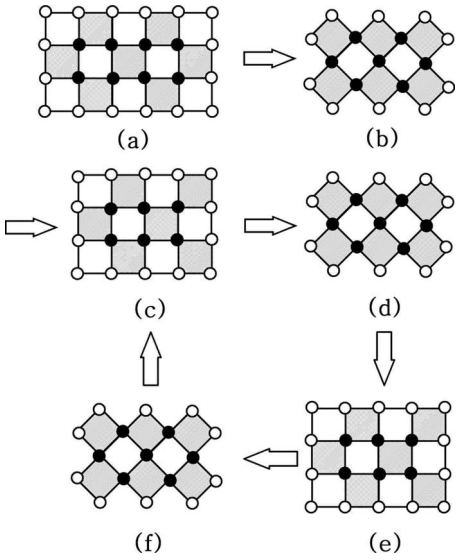

FIG. 8. A schematic plot of possible final configurations when calculating correlation functions with a separation $|\mathbf{r}_j-\mathbf{r}_i|=L=2^m$.

C. TERG algorithm on other lattice geometries

The detail implementation of TERG algorithm will be slightly different on other lattices. Here we discuss three other simple lattice geometries, namely, the honeycomb, Kagome, and triangle lattices. We would like to remark that the lattice geometry of TPS does not need to be the same as the lattice geometry of the physical model in generic cases.

1. Honeycomb lattice

On honeycomb lattice, we assume the tensors T_A and T_B in TPS to be different on sublattice A and B. As a result, the norm of the wave function can be represented as a tensor trace with two different double tensors $\mathbb{T}_A$ and $\mathbb{T}_B$ on sublattice A and B. To apply the TERG algorithm, we may first apply a basic move for two adjoint double tensors (see Fig. 9). Mathematically, the basic move in Fig. 9(a) is expressed as

$$\sum_{\gamma} \mathbb{T}^{A}_{\alpha\beta\gamma} T^{B}_{\mu\nu\gamma} \simeq \sum_{\gamma=1}^{D_{\text{cut}}} S_{A\nu\alpha\gamma} S_{B\beta\mu\gamma}. \tag{11}$$

This step can be realized by a SVD decomposition approximately.[23]

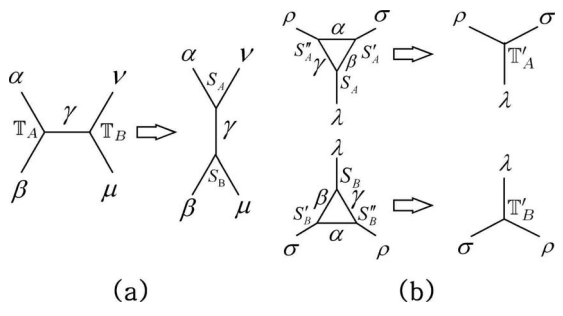

FIG. 9. The deformation and renormalization of double tensor $\mathbb{T}_{A(B)}$ on the honeycomb lattice.

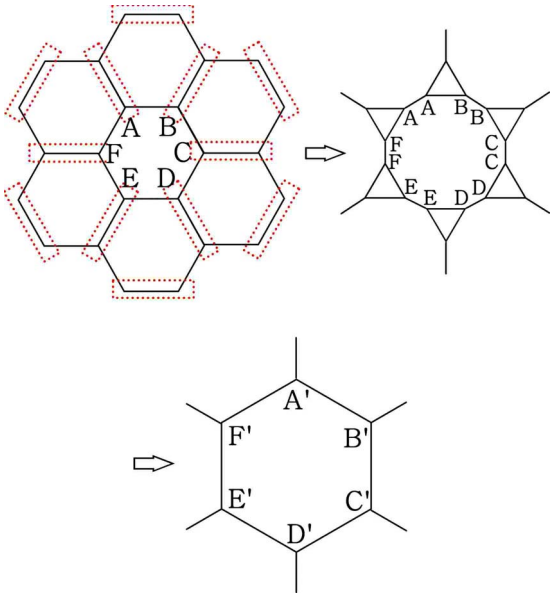

FIG. 10. (Color online) The tensor network on a honeycomb lattice with six impurity double tensors can also be coarse grained without generating more impurities.

By applying the basic move for all the links in the dashed boxes as shown in Fig. 10, we can deform the honeycomb tensor network into the triangle-honeycomb tensor network. Then we can sum over the inner links on each triangle and realize the coarse graining procedure. For example,

$$\mathbb{T}'_{A\lambda\sigma\rho} = \sum_{\alpha\beta\gamma} S_{A\beta\gamma\lambda} S'_{A\alpha\beta\sigma} S''_{A\gamma\alpha\rho}. \tag{12}$$

Similar on square lattice, this step is exact.

Again, the expectation value of a local Hamiltonian could also be represented by a contraction of tensor network with impurity double tensors. After coarse graining, the type of impurity tensors will also not increase. Simulating the tensor network with six impurity double tensors shown in Fig. 9(b) will allow us to evaluate up to six-body nearest-neighbor interactions (which include on-site interaction and nearest-neighbor, next-nearest-neighbor, next-next-nearest-neighbor two-body interactions as well as six-body plaquette interaction term on a hexagon).

2. Kagome and triangle lattices

The implementations of TERG algorithm on Kagome and triangle lattices can be very similar to honeycomb lattice. Actually, after one step lattice deformation, both of them can come to the case of honeycomb lattice. For simplicity, we consider the case of calculating a uniform tensor net.

Figure 11(a) shows that by decomposing rank-four double tensors on Kagome lattice into a summation of two rank-three tensors (the same as on square lattice, this step can be realized approximately by SVD decomposition), we can deform the Kagome lattice into triangle-honeycomb lattice, see in Figs. 11(b) and 11(c). Then by summing over the inner indices of each triangle, we end up with a honeycomb lattice geometry, see in Fig. 11(d).

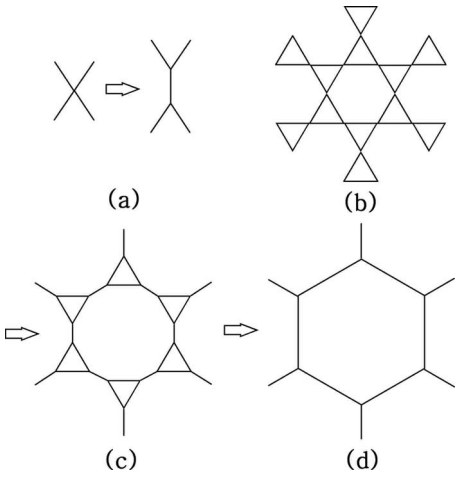

FIG. 11. A tensor network on Kagome lattice can be deformed into a tensor network on honeycomb lattice.

Figure 12(a) shows that by decomposing rank-six double tensors on triangle lattice into a summation of four rank-three tensors (this step can be realized approximately by several SVD decompositions as shown in Fig. 13), we can deform the triangle lattice into a geometry as shown in Fig. 12(c). Then again by summing over the inner indices of each triangle, we end up with a honeycomb lattice geometry [see Fig. 12(d)].

By applying the above geometry deformation and coarse graining procedure on tensor network (with and without impurities), we can also evaluate average energy and correlation functions for systems on Kagome and triangular lattices.

III. EXAMPLES OF SYMMETRY BREAKING PHASE TRANSITIONS

To test our TERG algorithm, we first calculate ground state and its magnetization along x and z directions for the transverse field Ising model,

$$H = -\sum_{\langle ij\rangle} \sigma_i^z \sigma_j^z - h\sum_i \sigma_i^x. \tag{13}$$

We choose the tensor T in Eq. (1) to be real and has 90° rotational symmetry. We also choose the inner dimension

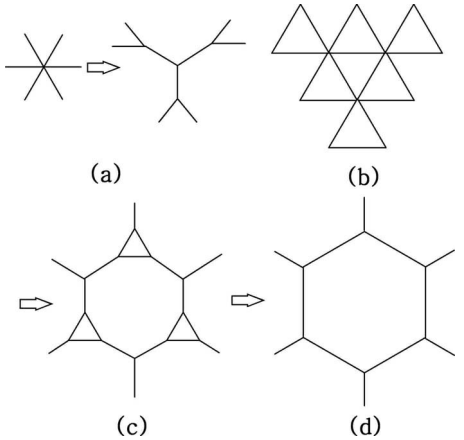

FIG. 12. A tensor network on triangular lattice can be deformed into a tensor network on honeycomb lattice.

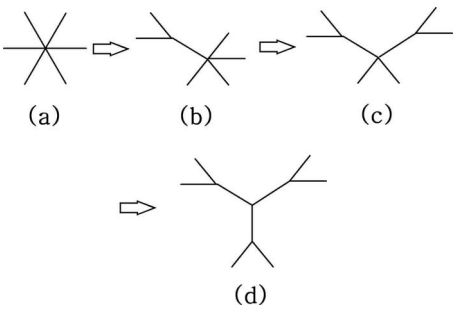

FIG. 13. A schematic plot of realizing the decomposition in Fig. 12(a) by several SVD decompositions.

$D=2$ and keep 18 singular values at each iteration ($D_{\text{cut}}=18$). The total system size is up to $2^9\times 2^9$ sites. The average energy for a tensor T is calculated using the TERG approach. We use Powell minimization method to find the minimal average energy and the corresponding tensor which gives us the variational ground state.

In Fig. 14 we plot the polarization along x and z directions in the variational ground state. We note that despite the $\sigma^z \to -\sigma^z$ symmetry in the Hamiltonian, the tensor T that minimize the average energy may break the $\sigma^z \to -\sigma^z$ symmetry and give rise to nonzero polarization in z direction. We find a second-order phase transition at $h_c \approx 3.08$. We further fit the critical exponent

$$\langle \sigma^z \rangle = A|h - h_c|^{\beta}, \tag{14}$$

with $\beta \approx 0.333 \pm 0.003$. Both the values of critical field and critical exponent β here are very close to the quantum Monte Carlo (QMC) results, with $h_c^{\text{QMC}} \simeq 3.044$ (Ref. 25) and $\beta^{\text{QMC}} \simeq 0.327$.[26] They are much better than the mean-field results $h_c=4$ and $\beta=0.5$.

To see the truncation error caused by D_{cut}, we plot the ground-state energy (per site) of Eq. (13) as a function of D_{cut}, for $h=2.8, 3.2$, and $h=h_c=3.08$ (see Fig. 15). The energies for different h's are shifted by different constants so that the three curves can be fitted into one window. Notice that for off-critical systems ($h=2.8, 3.2$), the energy converges very quickly for small D_{cut} (~ 26). Even at the critical point

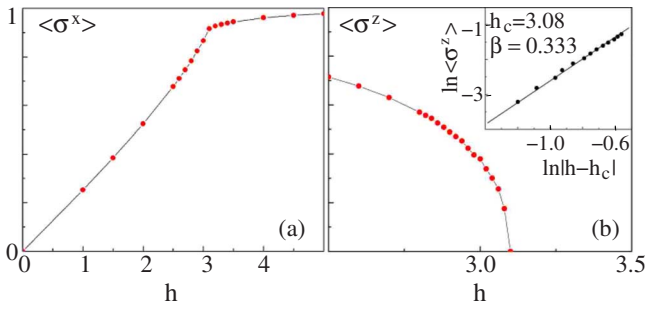

FIG. 14. (Color online) (a) Magnetization along the x direction $\langle \sigma^x \rangle$ versus transverse field h. The derivative of magnetization has a singularity around $h \simeq 3.1$, indicating the second-order phase transition. (b) Magnetization along the z direction $\langle \sigma^z \rangle$ versus transverse field h. In the inset is the log plot of $\langle \sigma^z \rangle$ versus $|h-h_c|$, where h_c is the critical field.

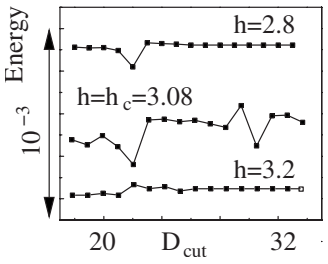

FIG. 15. Ground-state energies (with some constant shifts) of the transverse Ising model for different D_{cut}.

$h=h_c=3.08$, the error in energy per site is of order the 1×10^{-4}. The truncation error is much smaller for gapped off-critical states. Note that the nonmonotonic behavior of the error versus D_{cut} can be understood as there are both truncation errors in $\langle\Psi|\Psi\rangle$ and $\langle\Psi|h_i|\Psi\rangle$ and those errors are intrinsically random.

As another test, we also apply the TERG method to a gapless system—Heisenberg model: $H=\Sigma_{\langle ij\rangle}\boldsymbol{S}_i\cdot\boldsymbol{S}_j$ on square lattice. Here we choose $D=2,3$, or 4, $D_{\text{cut}}=18$, and total system size $2^9\times2^9$ sites. We choose tensors T_A and T_B to be real and has 90° rotational symmetry on sublattices A and B. We find the ground-state energy to be −0.330, −0.3323, and −0.3338 per bond for $D=2$, 3, and 4, which is quite close to the best QMC results −0.3350.[27,28] The TERG method also allows us to calculate correlation function using tensor network with two "impurity" tensors with arbitrary separations. Through the long-range correlation function, we find that the total magnetization is $m=\sqrt{\langle S_i^xS_j^x+S_i^yS_j^y+S_i^zS_j^z\rangle}=0.39$ for $D=2$, which is larger than the QMC results (0.307).[27,28] We see that a small error in ground-state energy (which depends only on short-range correlation) can lead to a larger error on correlations at long distances.

IV. EXAMPLES OF TOPOLOGICAL PHASE TRANSITIONS

In this section, we apply the TERG approach to a few models with string-net condensation. We calculate the phase diagram of these systems and study phase transitions from string-net condensed states to states without string-net condensation. These transitions are examples of continuous phase transitions between phases with different topological orders but the same symmetry.[8–13] As such, they are beyond the Landau symmetry breaking paradigm. Thus the TERG approach is capable of describing phases and phase transitions that cannot be described by Landau's symmetry breaking theory.

A. Z_2 gauge model

The first system that we study is a spin-1/2 system where the spins live on links of a square lattice. The Hamiltonian is given by

$$H=U\sum_v\left(1-\prod_{l\in v}\sigma_l^z\right)-g\sum_p\prod_{l\in p}\sigma_l^x-J\sum_l\sigma_l^z. \quad (15)$$

Here $\Pi_{l\in p}\sigma_l^x$ is the product of the four σ_l^x around a square p and Σ_p sums over all the squares. $\Pi_{l\in v}\sigma_l^z$ is the product of the four σ_l^z around a vertex v and Σ_v sums over all the vertices. Σ_l sums over all links. We will assume that $U=\infty$ and study the quantum phases of the above system as we change g and J. We will assume $J>0$ and $g>0$.

When $J=0$, Eq. (15) is exactly soluble.[29] To understand the exact ground state in the string language,[30] we interpret the $\sigma^z=-1$ and 1 states on a single link as the presence or absence of a string. The appropriate low-energy Hilbert space in large U limit is made of closed string states that satisfy $\Pi_{i\in v}\sigma_i^z=1$ at every vertex. The ground state is simply an equal weight superposition of all closed string states $|\Psi_{Z_2}\rangle=\Sigma_{X\in\text{closed}}|X\rangle$, which is called a string-net condensed state. Such a state is the simplest topologically ordered state.[31]

When $g=0$, the ground state is the spin-polarized state with no-down spins and no-closed strings. The above two states have the same symmetry. But due to the nontrivial topological order in the string-net condensed state, the two states belong to two different quantum phases. We would like to use the TERG approach to study the phase transition between the above two states with different topological orders.

We would like to mention that the low-energy effective theory of Eq. (15) is Z_2 gauge theory.[29,31,32] The transition between the string-net condensed and noncondensed phases is nothing but the transition between the deconfined and confined phases of Z_2 gauge theory.

One way to study such a phase transition is to introduce a variational wave function,

$$|\Psi_w\rangle=\sum_{X\in\text{closed}}w^{L_X}|X\rangle, \quad (16)$$

where L_X is the number of links on the string X. When $w=1$, $|\Psi_w\rangle$ becomes the string condensed state $|\Psi_{Z_2}\rangle$. When $w=0$, $|\Psi_w\rangle$ is the state with all spins in up direction which does not contain any strings. We see that w behaves like the string tension which controls the density of strings. $|\Psi_{w=1}\rangle$ is the ground state of Eq. (15) when $J=0$ and $|\Psi_{w=0}\rangle$ is the ground state of Eq. (15) when $g=0$.

Since $|\Psi_{w=1}\rangle$ and $|\Psi_{w=0}\rangle$ have the same symmetry, one might expect that as we change g/J, $|\Psi_{w=1}\rangle$ would change into $|\Psi_{w=0}\rangle$ smoothly and the ground-state energy of Eq. (15) would be a smooth function of g/J, implying that there was no quantum phase transition. In fact, we will see below that the ground-state energy of Eq. (15) is not a smooth function of g/J indicating that there is a quantum phase transition at a critical value $(g/J)_c$.

In order to calculate the energy expectation values in these states (and also to pave the way for generalizations) we write the trial wave function $|\Psi_w\rangle$ as a tensor-product state,

$$|\Psi_{Z_2}\rangle=\sum_{m_1,m_2,\ldots}\text{tTr}[\otimes_vT\otimes_lg^{m_l}]|m_1,m_2,\ldots\rangle, \quad (17)$$

where $m_l=0,1$ labels the up-spin and down-spin states on link l. To define the tensor trace, one can introduce a graphical representation of the tensors [see Fig. 16(a)]. Then tTr means summing over all indices on the connected links of tensor network. The variational state [Eq. (16)] that we introduced above is given by the following choice of tensors:

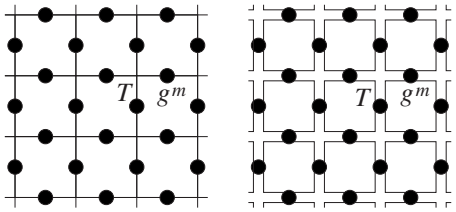

FIG. 16. (a) The spin-1/2 model Eq. (15) on links of a square lattice. The dots represent the physical spin states which are labeled by $m=0,1$. The above graph can also be viewed as a tensor network where each dot represents a rank-three tensor g and each vertex represents a rank-four tensor T. The two legs of a dot represent the α and β indices in the rank-three tensor $g^m_{\alpha\beta}$. The four legs of a vertex represent the four internal indices in the rank-four tensor $T_{\alpha\beta\gamma\lambda}$. The indices on the connected links are summed over which define the tTr. (b) A tensor network of the double-line tensors, where each dot represents a double-line tensor g and each vertex represents a double-line tensor T. The four legs of a dot represent the $\alpha_{1,2}$ and $\beta_{1,2}$ indices in the tensor $g^m_{\alpha_1\alpha_2;\beta_1\beta_2}$. The eight legs of a vertex represent the internal indices in the rank-four tensor $T_{\alpha_1\alpha_2;\beta_1\beta_2;\gamma_1\gamma_2;\lambda_1\lambda_2}$. The indices on the connected links are summed over which define the tTr.

$$T_{\alpha\beta\gamma\delta}=\begin{cases}1 & \text{if } \alpha+\beta+\gamma+\delta \text{ even}\\ 0 & \text{if } \alpha+\beta+\gamma+\delta \text{ odd},\end{cases} \tag{18}$$

$$g^0_{00}=1, \quad g^1_{11}=w, \quad \text{others}=0, \tag{19}$$

with internal indices like α running over 0 and 1. The rank-3 tensor g behaves like a projector which essentially sets the internal index equal to the physical index so that $\alpha=1$ represents a string and $\alpha=0$ represents no string. The meaning of the tensor $T_{\alpha\beta\gamma\delta}$ is also clear; it just enforces the closed string constraint, only allowing an even number of strings to meet at a vertex.

Once we have expressed the trial wave function as a TPS, we can use the TERG method to calculate the average energy in a very efficient way[33] and minimize the average energy by varying w. The resulting (minimized) average energy as a function of g/J is plotted in Fig. 17. From the discontinuity in the slope, we see that there is a first-order phase transition at $g/J\approx 2.3$ between the two states with and without string-net condensation (see Fig. 19).

How good is this result? On a quantitative level, it is not very good: the phase transition is known to occur at $(g/J)_c \approx 3.044$.[25] However, this is not surprising since we used the simplest possible variational wave function. We expect the estimate for $(g/J)_c$ to improve when we increase the number of variational parameters—for example, by considering g and T with larger dimension.

A more serious problem is that the result is wrong on a qualitative level: the phase transition is known to be of second order not first order. This problem cannot be overcome by blindly generalizing the tensors g and T. Instead, we have to choose these tensors in a special way. To understand the basic issue, let us consider another set of variational tensors. In this scheme, the internal indices for the T and g tensors

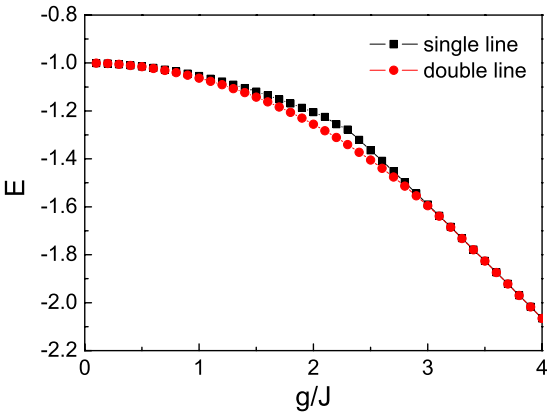

FIG. 17. (Color online) The black squares are (minimized) average energies of the Z_2 model (15) for the single-line tensor network Eqs. (18) and (19)]. The red dots are (minimized) average energies for the double-line tensor network [Eqs. (22) and (21)]. (Here again we choose $D_{\text{cut}}=18$ and total system size is $2^9\times 2^9$)

still run from 0 to 1, but each leg now has two internal indices, see in Fig. 18,

$$T_{\alpha\beta\gamma\lambda}=T_{\alpha_1\alpha_2;\beta_1\beta_2;\gamma_1\gamma_2;\lambda_1\lambda_2}=T^0_{\alpha_1\beta_1\gamma_1\lambda_1}\delta_{\alpha_2\gamma_1}\delta_{\gamma_2\beta_2}\delta_{\beta_1\lambda_2}\delta_{\lambda_1\alpha_1} \tag{20}$$

with $\alpha_1,\alpha_2,\beta_1,\beta_2,\gamma_1,\gamma_2,\lambda_1,\lambda_2=0,1$ and

$$g^0_{11,11}=g^0_{00,00}=1, \quad g^1_{10,10}=g^1_{01,01}=1, \quad \text{others}=0. \tag{21}$$

In such constructions, our tensors have a double-line structure [see Fig. 16(b)]. Again, g^m are projectors that relate the internal indices with physical indices. Here, on each leg of g and T tensors, the double line with the same value is projected to the spin-up state and the double line with different values is projected to the spin-down state.

To maintain the 90° rotational symmetry, we choose T^0 to have the form (assuming $T^0_{1111}=1$)

$$x(1)=T^0_{0000},$$

$$x(2)=T^0_{0111}=T^0_{1011}=T^0_{1101}=T^0_{1110},$$

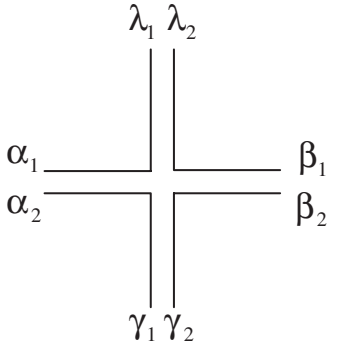

FIG. 18. The graphic representation for the double-tensor ansatz in Eq. (20).

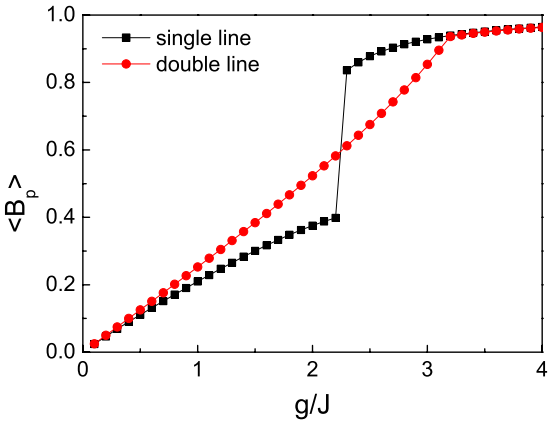

FIG. 19. (Color online) $\langle B_p \rangle$ versus g/J. The single-line variational wave function shows a jump in $\langle B_p \rangle$, which indicates a first-order phase transition around $g/J=2.3$ (black squares). The double-line variational wave functions have no jump in $\langle B_p \rangle$ but the discontinuity in the derivative indicates a second-order phase transition around $g/J=3.2$ (red dots).

$$x(3) = T^0_{1000} = T^0_{0100} = T^0_{0010} = T^0_{0001},$$

$$x(4) = T^0_{1100} = T^0_{0011} = T^0_{0110} = T^0_{1001},$$

$$x(5) = T^0_{1010} = T^0_{0101}. \tag{22}$$

We note that for such a choice of T^0 and g^m, the trial wave function contains only closed string states.

Using the TERG approach to minimize the average energy, we find the variational ground-state energy which is plotted in Fig. 17. We find that there is a phase transition between the two phases with and without string-net condensation. But now the phase transition is a second-order phase transition at $g/J \approx 3.2$ (see Fig. 19). Note that this result is better than our previous result both quantitatively and qualitatively.

The quantitative improvement is perhaps not surprising since we are using more variational parameters. A more important issue is that the double-line mean-field theory correctly describes a second-order phase transition, while the single-line mean-field theory did not. Why is this?

Note that there is a Z_2 redundancy in the double-line tensors (like the gauge redundancy in gauge theory). As we exchange values of 0 and 1 for all the internal indices of the double-line tensors, we induce a Z_2 transformation on those double-line tensors: $(T, g^m) \to (\tilde{T}, \tilde{g}^m)$. However, such a Z_2 transformation does not change the physical wave function: $\mathrm{tTr}[\otimes_v T \otimes_l g^{m_l}] = \mathrm{tTr}[\otimes_v \tilde{T} \otimes_l \tilde{g}^{m_l}]$. Thus (T, g^m) and $(\tilde{T}, \tilde{g}^m)$ are two labels that label the same physical state.

The variational approach used here is similar to calculating an average in a local classical statistical system. The presence of a Z_2 symmetry allows a classical system to have a Z_2 symmetry breaking transition which is a second-order phase transition. This is the reason why the double-line tensors are capable of producing a second-order phase transition. In contrast, for the single-line tensors, the corresponding classical system does not have any symmetry and, as a result, it cannot describe a second-order transition.

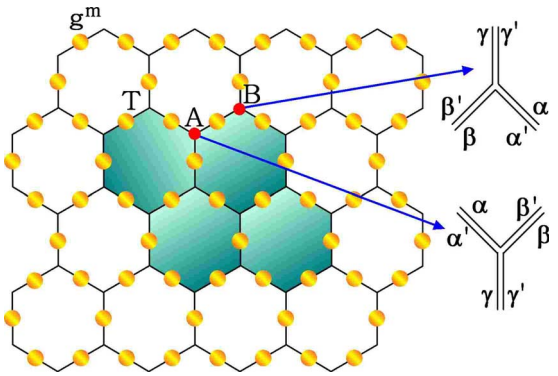

FIG. 20. (Color online) The double-semion model on the honeycomb lattice. The ground-state wave function (26) has a TPS representation given by the above tensor network. Note that T and g has a double-line structure. The vertices form a honeycomb lattice which can be divided into A and B sublattices.

We would like to mention that there is a duality transformation that relate the 2D Z_2 gauge theory to transverse field Ising model.[34] Such a duality mapping allows us to relate the phase transition between the deconfined and confined phases of the Z_2 gauge theory to the spin-ordered and disordered transitions in the transverse field Ising model. This is how we know that the transition between the string-net condensed and noncondensed phases is a second-order phase transition and that it occurs at critical coupling $g/J \approx 3.044$. In fact, the double-line tensors exactly realize the duality mapping between the 2D Z_2 gauge theory and transverse field Ising model. From the structure of the double tensors in Eqs. (21) and (22), we see that each square loops in Fig. 16(b) carries the same value of internal indices, which correspond to the value of a dual spin (located at the center of the square) in the dual Ising model. The string formed by the down spins on the links corresponds to a domain wall in the dual Ising model.

B. Double-semion model

Next we consider a more complicated model where spins are located on the links of a honeycomb lattice (see Fig. 20),

$$H = U \sum_{\boldsymbol{I}} \left(1 - \prod_{\text{legs of } \boldsymbol{I}} \sigma^z_i \right) - J \sum_{\boldsymbol{i}} \sigma^z_{\boldsymbol{i}} - g \sum_{\boldsymbol{p}} \left(\prod_{\text{edges of } \boldsymbol{p}} \sigma^x_j \right) \times \left(\prod_{\text{legs of } \boldsymbol{p}} i^{1-\sigma^z_j/2} \right), \tag{23}$$

where $\boldsymbol{i}$ labels the links, $\boldsymbol{I}$ labels the vertices, and $\boldsymbol{p}$ labels hexagons. Again we consider $U=\infty$ limit.[35] When $J=0$, the above model is exactly soluble and the exact ground state is given by[21] $|\Psi_{\text{sem}}\rangle = \Sigma_X (-)^{l(X)} |X\rangle$, where Σ_X sums over all the closed string configurations and $l(X)$ is number of closed loops in X. The ends of string in such a state have the semion statistics. When $g=0$, the model is also exactly soluble and the spins all point up (i.e. no strings) in the ground state.

To study the phase transition between the above two states, again we choose the double-line tensors to construct

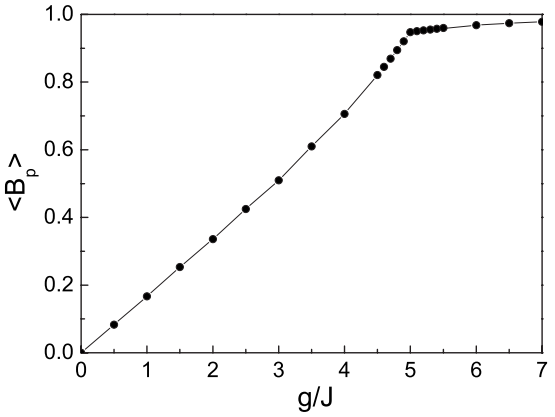

FIG. 21. $\langle B_p \rangle$ versus g/J; the discontinuity of the derivative around $g/J=5.0$ indicates a second-order confinement-deconfinement phase transition. (Here again we choose $D_{\text{cut}}=16$ and total number of lattice sites is 2×3^{15}.)

the trial wave function (see Fig. 20). The T tensors in the vertices are given schematically by

$$\text{sublattice A:} \quad T_{\alpha\alpha';\beta\beta';\gamma\gamma'} = T^A_{\alpha\beta\gamma}\delta_{\alpha\beta'}\delta_{\beta\gamma'}\delta_{\gamma\alpha'},$$

$$\text{sublattice B:} \quad T_{\alpha\alpha';\beta\beta';\gamma\gamma'} = T^B_{\alpha\beta\gamma}\delta_{\alpha'\beta}\delta_{\beta'\gamma}\delta_{\gamma'\alpha}, \quad (24)$$

where each internal index represented by one of the double lines runs over 0 and 1. The tensors T^A and T^B are given by

$$x(1) = T^A_{011} = T^A_{101} = T^A_{110}; \quad x(2) = T^A_{001} = T^A_{100} = T^A_{010},$$

$$x(3) = T^A_{111}, \quad x(4) = T^A_{000},$$

$$x(5) = T^B_{011} = T^B_{101} = T^B_{110}, \quad x(6) = T^B_{001} = T^B_{100} = T^B_{010},$$

$$x(7) = T^B_{111}, \quad x(8) = T^B_{000}. \quad (25)$$

The g tensors on the links are given by Eq. (21). The trial wave function is obtained by summing over all the internal indices on the connected links in the tensor network (see Fig. 20),

$$|\Psi_{\text{dsemion}}\rangle = \sum_{\{m_l\}} \text{tTr}[\otimes_v T \otimes_l g^{m_l}]|m_1, m_2, \ldots\rangle. \quad (26)$$

Again, the physical indices and the internal indices have a similar relation as in the Z_2 double-line tensors. When $x(1)=x(5)=-i$, $x(2)=x(6)=i$, and $x(3)=x(4)=x(7)=x(8)=1$, the tensor reproduces the right sign oscillations $(-)^{l(X)}$ essentially by counting the number of left and right turns made by the string.

We used the TERG approach to find the variational ground states for different g/J. The detailed implementation is a little different from the square lattice, as shown in Figs. 9 and 10. Then we used the TERG approach to calculate $\langle B_p \rangle$ for those variational ground states with minimized energies. The result is presented in Fig. 21. We see that there is a second-order phase transition at $g/J \approx 5.0$, which should correspond to the transition between the string-net condensed and noncondensed states. This agrees with the Monte Carlo result where a second-order phase transition appears at $(g/J)_c \approx 4.768$.[25] (Note that in the infinite U limit, the above model is equivalent to the usual Z_2 gauge model on honeycomb lattice by applying a global unitary mapping, which is dual to the transverse Ising model on triangle lattice.)

V. CONCLUSION

The TERG approach is a generic method to obtain various quantum phases and quantum phase transitions for 2D quantum systems. The most important feature of TERG approach is that it can handle quantum states with long-range entanglement (such as topologically ordered states). When we use traditional mean-field theory to calculate a quantum phase diagram, the topological ordered phases cannot appear in such a mean-field phase diagram since the mean-field states are limited to those with short-range entanglement. The TERG approach solves this problem and can generate phase diagrams that contain both symmetry breaking states and topologically ordered states. Thus the TERG approach may play a role for topologically ordered states analogous to the Ginzburg-Landau theory for symmetry breaking states.

We have seen that to use the TERG approach to study topological phases and topological phase transitions, one needs to choose the variational tensors carefully. An important question is how to choose the tensors in more general situations. One hint is that all the string-net states constructed in Ref. 21 can be expressed naturally in terms of a generalization of the double-line tensor network, which involves triple-line tensors.[22] This triple-line tensor network may correspond to the dual representation of the string-net states and may correspond to a suitable choice for the variational TERG approach. This may lead to a systematic variational approach for topological phases and topological phase transitions.

We would like to remark that the variational ansatz with small D often does not produce good long-range correlation functions even though the local energy can be very good (which is shown in the example of square Heisenberg model). Actually, this is a common weakness suffered by any kind of variational method, such as VQMC, DMRG. However, by using better global minimizing methods, we can increase D from $D=2$ used in this paper to a larger value which will produce better results and eliminate the above weakness. This will be part of our future work. Other spin models, such as Heisenberg model on Kagome lattice and J_1-J_2 model, are more interesting physically and the results will be presented in future publications.

Finally we would like to mention that the TERG variational method may also be useful in analyzing interacting fermion models since these models can be mapped back to local spin models.[36–38] Indeed, in Sec. IV we already saw examples of models with fermion and anyon excitations which could be studied by the TERG method.

ACKNOWLEDGMENTS

We would like to thank Frank Verstraete for very helpful discussions and comments. This research was supported by

the Foundational Questions Institute (FQXi) and NSF under Grant No. DMR-0706078.

APPENDIX: SCALING OF ERRORS IN SEVERAL VARIATIONAL METHODS

In a VQMC calculation, the error ϵ is a statistical error that scales like $1/N^{1/2}$ where N is the number of samples. The computational time T scales like N. Thus the scaling of the error with computational time is given by $\epsilon \sim 1/T^{1/2}$.

In the 1D approach, the error ϵ is a finite-size error that comes from the truncation of the infinite 2D lattice to an $L \times \infty$ lattice. In a gapped system we expect this error to fall off as $e^{-L/\xi}$ where ξ is the correlational length. On the other hand, the computational time T is exponential in L since the method requires diagonalizing a transfer matrix whose size is exponentially large in L. We conclude that the error scales with the computational time as $\epsilon \sim e^{-\text{const}(\log T)}$.

In the TERG approach, the truncation error for each iteration step scales as $\epsilon_1 \sim e^{-\text{const}(\log D_{\text{cut}})^2}$, since calculating the norm and averages is like calculating the partition function in Ref. 23. The total truncation error for a system of size L is $\epsilon_t \sim (\log L) e^{-\text{const}(\log D_{\text{cut}})^2}$ since such a system requires $\log L$ iterations. On the other hand, the finite-size error is $\epsilon_s \sim e^{-L/\xi}$. Minimizing the sum of the two errors, we see that the optimal L is given by $L \sim (\log D_{\text{cut}})^2$. Since the computational time scales polynomially in D_{cut}, we conclude that the total error scales like $\epsilon \sim e^{-\text{const}(\log T)^2}$ (neglecting subleading log corrections).

[1] L. D. Landau, Phys. Z. Sowjetunion **11**, 26 (1937).
[2] L. D. Landau and E. M. Lifschitz, *Statistical Physics*, Course of Theoretical Physics Vol. 5 (Pergamon, London, 1958).
[3] V. L. Ginzburg and L. D. Landau, Zh. Eksp. Teor. Fiz. **20**, 1064 (1950).
[4] X.-G. Wen, Adv. Phys. **44**, 405 (1995).
[5] X.-G. Wen, Phys. Lett. A **300**, 175 (2002).
[6] A. Kitaev and J. Preskill, Phys. Rev. Lett. **96**, 110404 (2006).
[7] M. Levin and X.-G. Wen, Phys. Rev. Lett. **96**, 110405 (2006).
[8] X.-G. Wen and Y.-S. Wu, Phys. Rev. Lett. **70**, 1501 (1993).
[9] W. Chen, M. P. A. Fisher, and Y.-S. Wu, Phys. Rev. B **48**, 13749 (1993).
[10] T. Senthil, J. B. Marston, and M. P. A. Fisher, Phys. Rev. B **60**, 4245 (1999).
[11] N. Read and D. Green, Phys. Rev. B **61**, 10267 (2000).
[12] X.-G. Wen, Phys. Rev. Lett. **84**, 3950 (2000).
[13] X.-G. Wen, Phys. Rev. B **65**, 165113 (2002).
[14] M. Levin and X.-G. Wen, Phys. Rev. B **75**, 075116 (2007).
[15] F. Verstraete and J. I. Cirac, arXiv:cond-mat/0407066 (unpublished).
[16] F. Verstraete, M. M. Wolf, D. Perez-Garcia, and J. I. Cirac, Phys. Rev. Lett. **96**, 220601 (2006).
[17] M. Aguado and G. Vidal, Phys. Rev. Lett. **100**, 070404 (2008).
[18] J. Jordan, R. Ors, G. Vidal, F. Verstraete, and J. I. Cirac, arXiv:cond-mat/0703788 (unpublished).
[19] S. R. White, Phys. Rev. Lett. **69**, 2863 (1992).
[20] S. Östlund and S. Rommer, Phys. Rev. Lett. **75**, 3537 (1995).
[21] M. A. Levin and X. G. Wen, Phys. Rev. B **71**, 045110 (2005).
[22] Z.-C. Gu, M. Levin, B. Swingle, and X.-G. Wen, arXiv:0809.2821 (to be published).
[23] M. Levin and C. P. Nave, Phys. Rev. Lett. **99**, 120601 (2007).
[24] G. Vidal, Phys. Rev. Lett. **99**, 220405 (2007).
[25] H. W. J. Blote and Y. Deng, Phys. Rev. E **66**, 066110 (2002).
[26] A. Pelissetto and E. Vicari, Phys. Rep. **368**, 547 (2002).
[27] A. W. Sandvik, Phys. Rev. B **56**, 11678 (1997).
[28] A. W. Sandvik and H. G. Evertz, arXiv:0807.0682 (unpublished).
[29] A. Y. Kitaev, Ann. Phys. (N.Y.) **303**, 2 (2003).
[30] X.-G. Wen, *Quantum Field Theory of Many-Body Systems—From the Origin of Sound to an Origin of Light and Electrons* (Oxford University Press, Oxford, 2004).
[31] X.-G. Wen, Phys. Rev. B **44**, 2664 (1991).
[32] N. Read and S. Sachdev, Phys. Rev. Lett. **66**, 1773 (1991).
[33] We can absorb the g tensor into the T tensor when we construct the double tensor in the TERG calculation.
[34] J. B. Kogut, Rev. Mod. Phys. **51**, 659 (1979).
[35] More seriously, the above expression for the double-semion model only valid in the infinite U limit and we need a more complicated Hamiltonian for generic U (Ref. 21). This is because the Hermitian condition for the last term is only correct in the closed string subspace.
[36] M. Levin and X.-G. Wen, Phys. Rev. B **67**, 245316 (2003).
[37] R. C. Ball, Phys. Rev. Lett. **95**, 176407 (2005).
[38] F. Verstraete and J. Cirac, J. Stat. Mech.: Theory Exp. 2005, 12.